PHYSICAL REVIEW D **94,** 016004 (2016)

High resolution nonperturbative light-front simulations of the true muonium atom

Henry Lamm* and Richard F. Lebed†

Department of Physics, Arizona State University, Tempe, Arizona 85287, USA

(Received 27 June 2016; published 28 July 2016)

Through the development of a parallel code called TMSWIFT, an extensive light-front quantization study of the nonperturbative spectrum of the bound state $(\mu^+\mu^-)$, true muonium, has been performed. Using Padé approximants, it has been possible to extract continuum and infinite-cutoff limits for the singlet and triplet states for a range of values of the coupling constant α. This data set allows for an investigation of the α dependence of the light-front spectra, the results of which are compared to standard calculations. Decay constants have also been obtained. Improved calculations have been undertaken for the energy shifts due to the presence of a second, lighter flavor (e). Finally, initial results for three-flavor (e, μ, τ) calculations are presented.

DOI: 10.1103/PhysRevD.94.016004

I. INTRODUCTION

True muonium is the as-yet undiscovered $(\mu^+\mu^-)$ bound state. Its spectrum, with lifetimes in the range of picoseconds to nanoseconds [1], is well defined since the 2.2 μs weak-decay lifetime of the muon is much longer. The levels and transitions of true muonium are dominated by QED effects because its purely leptonic nature relegates the influence of QCD to vacuum polarization, where it contributes a small effect at $\mathcal{O}(\alpha^5)$ [2,3]. Electroweak effects are suppressed further and become relevant only when all $\mathcal{O}(\alpha^7)$ terms are considered [4]. The existing discrepancies in muon physics [the muon anomalous magnetic moment $(g-2)_\mu$ [5], the proton charge radius r_P [6], $B^+ \to K^+\ell^+\ell^-$ decays [7], $\bar{B}^0 \to D^{*+}\ell^-\bar{\nu}_\ell$ [8]] motivate a serious investigation of true muonium, which has been shown to have strong discriminating power among alternative resolutions to these anomalies [4,9–11]. Using the methods developed in this paper, nonperturbative corrections to bound states from these new physics proposals could be investigated through the inclusion of new matrix elements, allowing for more stringent constraints than those obtained through conventional perturbative studies.

The atom's nonobservation to date is due to difficulties in producing associated low-energy muon pairs, as well as its short lifetime. Many proposed methods of production exist [1,12–20]. The Heavy Photon Search (HPS) experiment in 2016 will begin a search for true muonium at a fixed target [19,21]. Additionally, the DImeson Relativistic Atom Complex (DIRAC) might observe the atom in an upgraded run [22,23]. Given enough statistics, DIRAC could obtain a value for the Lamb shift using methods developed for $(\pi^+\pi^-)$ [24]. These experiments produce relativistic true muonium: In general, the μ^+ and μ^- are produced relativistically, both with respect to the lab frame and each other. Unfortunately, instant-form (conventional fixed-time) wave functions are not functions of boost-invariant variables (because the μ^+ and μ^- rest frames are not the same); thus, production and decay rates can be modified. To reduce this uncertainty, we produce boost-invariant wave functions through light-front techniques [25,26].

To establish the context for the work presented here, a discussion of the history of this and related problems is appropriate. Weinberg, interested in the *infinite-momentum frame* (in which a state's momentum component $p_z \to \infty$), discovered in the case of the ϕ^3 theory that creating or annihilating particles from the vacuum was forbidden [27]. This observation eventually led to the understanding that the vacuum of such a field theory is trivial (i.e., empty of ordinary particles), and that Fock states with fixed particle content are well defined. Instead of taking the infinite-momentum limit of instant-form field theory, one can obtain equivalent results by quantizing at fixed values of light-front time $x^+ \equiv t + z$ (called *front form*) [28]. In front form, one is able to develop a rigorous, closed-form Hamiltonian formalism [29]. In this formalism, an analogue of the Schrödinger equation exists, since an infinite but denumerable set of coupled integral equations for eigenstates of the Hamiltonian occurs. The front form admits a perturbation theory, and its Feynman rules were derived by Kogut and Soper [30]. Because of the inequivalent nature of instant-form and front-form quantization, it has been a crucial, but highly nontrivial, matter to show that the traditional instant-form calculations give equivalent results to those from the front form [31–39].

Perturbative front-form methods have shown success in the study of non-Abelian gauge theories. In QCD, these methods have been used to obtain results for exclusive processes by Lepage and Brodsky [40], where equivalent

*hlammiv@asu.edu
†Richard.Lebed@asu.edu

instant-form expressions did not exist. Analytical results using light-front techniques have also reproduced the correct leading-order Lamb shift and hyperfine splitting (HFS) for QED bound states [41–44]. The Yukawa theory has been used to understand the differences between instant-form and front-form approaches and how they can be reconciled [35,38,45–47]. The complete standard model has also been formulated in light-front quantization [48].

As mentioned, the existence of a closed-form Hamiltonian allows for a Schrödinger-like equation that can be expressed in an infinite-dimensional Fock space, which can be used to solve nonperturbative field theory, and allows techniques from nonrelativistic quantum mechanics to be applied to quantum field theory. To make these problems tractable, the infinite set of coupled equations must be truncated in a suitable way. In analogy to results in instant form, these truncations can produce divergent results and must be regularized to obtain sensible answers. The topic of how to renormalize such a Hamiltonian was first considered in [49]. One method proceeds by truncating the Fock space to a finite number of states based on particle content. In this truncation, renormalization is possible through Fock state sector-dependent counterterms [46,47,50–55], Pauli-Villars regulators [56–60], or the use of flow equations [61–64]. While each method works in principle, the practical difficulty of renormalizing nonperturbative Hamiltonians remains daunting.

In order to solve these field theories numerically, the Fock states are furthermore discretized in momentum Fourier modes on a lattice, a method called discretized light cone quantization (DLCQ). This method was pioneered by Pauli and Brodsky, working with a $(1+1)$-dimensional Yukawa theory [65]. The special feature of superrenormalizability of field theories in $1+1$ has been particularly amenable to DLCQ, and these theories have been investigated in depth. Sawicki used the method to solve scalar QED_{1+1} [66,67], while Harindranath and Vary investigated the structure of the vacuum and bound states of ϕ^3_{1+1} and ϕ^4_{1+1} models [68–70]. Pushing further, Hornbostel *et al.* presented results for the meson and baryon eigenstates of QCD_{1+1} [71], while Swenson and Hiller studied more field-theoretical properties of the light front in the Wick-Cutkosky model [72]. The Schwinger model, which admits analytical solutions in both instant form and front form, was first studied by Eller *et al.* in 1986 [73], and since has become an important test bed for developing improvements that can then be used in other theories [74–81].

Since DLCQ produces both the wave functions and the energy levels, Hiller was able to compute the R ratio in QED_{1+1} [82]. In one spatial dimension, DLCQ has also been applied to solving 't Hooft's model of large-N QCD [83], adjoint QCD [84–86], and supersymmetric models [87–97]. Although spontaneous symmetry breaking is manifested in a distinctly different way in $1+1$, it is also possible to study using DLCQ [98–100]. Finally, research has been undertaken using DLCQ to test Maldecena's AdS/CFT conjecture in $1+1$ theories [95,101].

Extending DLCQ beyond $1+1$ dimensions is complicated in two ways: first, higher-dimensional theories require regularization and renormalization, as discussed above. Second, the number of Fock states grows so rapidly that tractable numerical calculations allow only a small number of states to be included. Despite these difficulties, DLCQ was applied first to positronium by Tang *et al.* [102]. In that work, the effective Hamiltonian matrix equation was derived for a model including only the $|e^+e^-\rangle$ and $|e^+e^-\gamma\rangle$ Fock states. Variational methods were applied to this effective model and produced upper limits on the triplet state. Attempts to apply DLCQ to QCD were undertaken at the same time by Hollenberg [103], but renormalization and computational resources prevented much success. Further developments in understanding the connection between light-front and instant-form techniques were studied by Kaluža and Pauli, reproducing the expected results for the HFS and Bohr states in the limit of $\alpha \to 0$ [104]. Krautgärtner *et al.*, implementing the *Coulomb counterterm* techniques developed by Wölz [105], solved the effective matrix equation for positronium [106]. They found that it was possible to reproduce the correct Bohr spectrum, as well as the leading relativistic HFS, for both $\alpha_{\mathrm{QED}} = 1/137$ and $\alpha = 0.3$, albeit with some cutoff dependence. Concerned with the effect of *zero modes* (nontrivial field configurations in the Fock vacuum), Kalloniatis and Pauli undertook numerical simulations based upon perturbative solutions to the zero-mode constraint equations [107].

Krautgärtner further developed these techniques and began to analytically study the two-photon exchange interaction and its relationship to the observed divergences in his dissertation [108]. Wölz, in his dissertation, applied DLCQ to QCD by including the $|q\bar{q}gg\rangle$ Fock state [109]. Numerical limitations at the time prevented implementation of the counterterm techniques being concurrently developed, so that a slow convergence in the number of discretization points and a strong dependence on the momentum cutoff precluded these results from suggesting any conclusive statements. Synthesizing all these techniques, Trittmann computed the first results for positronium with the inclusion of the annihilation $e^+e^- \to \gamma$ channel [110–112]. Utilizing the good quantum number J_z, he was able to split the problem into sectors and investigate the breaking of rotational invariance inherent in light-front form in the effective equation. Cutoff dependence and inadequate computational resources were the major limits to Trittmann's work. With improved computing resources and the introduction of a special counterterm to cancel a divergent matrix element, DLCQ was applied by the current authors to two-flavor QED to obtain bound states

of positronium and true muonium simultaneously [25]. This work built upon the prior methods by incorporating a number of features of QED bound states in front-form field theory.

Beyond DLCQ, other numerical methods have been developed for light-front systems. Basis light-front quantization (BLFQ) follows from discretizing the momenta into harmonic-oscillator modes in the transverse direction instead of using Fourier modes. This method aspires to decrease the number of basis states needed by more accurately representing the functional behavior of the wave function. BLFQ has shown initial success in solving bound-state problems in QED [113–119] and QCD [120]. Using Monte Carlo methods developed for instant-form lattice gauge theory, transverse lattice theory has investigated simple models of QCD in $3+1$ dimensions [121–124]. Tube-based, collinear QCD and other effective-Hamiltonian methods also exist [125–127]. In recent years, the AdS/QCD conjecture has been extended to light-front field theory to produce the low-energy meson and baryon spectra [128–137].

The limitations of Fock-state truncation in renormalization have also prompted the study of other methods of truncation. Drawing upon the techniques found in many-body physics, coupled-cluster [138–140] and coherent-basis truncations [37,141–145] have shown promise in simpler systems.

This paper is organized as follows. In Sec. II we briefly review the model of true muonium studied here. Section III is devoted to presenting the numerical results obtained for the energy levels and the decay constants, with emphasis on the effect of the annihilation channel and of the presence of multiple flavors on the states. We conclude in Sec. IV with some discussion of our results and possible directions for future work.

II. TRUE MUONIUM MODEL

We review here the major points of our model, which are described in detail in a previous work [25]. In front form, the eigenvalue equation for a bound state is given by

$$\left(M^2-\sum_i\frac{m_i^2+\boldsymbol{k}_{\perp i}^2}{x_i}\right)\psi(x_i,\boldsymbol{k}_{\perp i};h_i)=\sum_{h_j}\int_D \mathrm{d}x_j'\mathrm{d}^2\boldsymbol{k}_{\perp j}'\langle x_i,\boldsymbol{k}_{\perp i};h_i|V_{\mathrm{eff}}|x_j',\boldsymbol{k}_{\perp j}';h_j\rangle\times\psi(x_j',\boldsymbol{k}_{\perp,j}';h_j),\tag{1}$$

where M is the invariant mass of the state, m indicates a mass term, i, j are component particle indices, x and $\boldsymbol{k}_\perp$ are the conventional longitudinal and transverse momentum light-front coordinates, respectively, h is shorthand for all intrinsic quantum numbers of a state, and V_{eff} are interaction terms given by the light-front Hamiltonian. The domain D of Eq. (1) is made well defined by the introduction of cutoff Λ, and we choose [40]

$$\frac{m^2+\boldsymbol{k}_\perp^2}{x(1-x)}\le\Lambda^2+4m^2.\tag{2}$$

Our model considers only the truncated Fock space of $|\ell_i\bar{\ell}_i\rangle$, $|\ell_i\bar{\ell}_i\gamma\rangle$, and $|\gamma\rangle$. The single-photon interaction allows for mixing between flavors via the annihilation channel. The wave functions are in the form of helicity states only for pure lepton states (e.g., $|\mu^+\mu^-\rangle$). The $|\gamma\rangle$ and $|\ell_i\bar{\ell}_i\gamma>$ components are folded into V_{eff} by means of the method of iterated resolvents [110,146].

Discretization in $(x,\boldsymbol{k}_\perp)$ space results in an asymmetric matrix in the discretized form of Eq. (1), which significantly increases the computational effort, so instead it is numerically superior to use the polar coordinates utilized initially by Karmanov [147] to study a toy model of the deuteron, and later by Sawicki [66,67] to study relativistic scalar-field bound states on the light front. These coordinates are defined by

$$x=\frac{1}{2}\left(1+\frac{\mu\cos\theta}{\sqrt{m_i^2+\mu^2}}\right),\tag{3}$$

$$\boldsymbol{k}_\perp=\mu(\sin\theta\cos\phi,\sin\theta\sin\phi,0).\tag{4}$$

Using these variables, one may exchange ϕ for the discrete quantum number J_z [110] and compute using only μ,θ. The new variable μ can be considered an off-shell momentum, due to the relation

$$\frac{m_i^2+\boldsymbol{k}_\perp^2}{x(1-x)}=4(\mu^2+m_i^2).\tag{5}$$

Since these coordinates depend upon the fermion mass m_i, different sets of μ, θ values result from the same sets of x and $\boldsymbol{k}_\perp$ values in the multiple-flavor system.

It has been shown [25,106,110] that strong dependence in ${}^1S_0$ states on Λ arises from the matrix element between antiparallel-helicity states called G_2. In the limit of $k_\perp\equiv|\boldsymbol{k}_\perp|$ or $k_\perp'\equiv|\boldsymbol{k}_\perp'|\to\infty$, this interaction approaches

$$\lim_{k_\perp\to\infty}G_2=-\frac{\alpha}{\pi}\frac{2}{x+x'-2xx'}\delta_{J_z,0},\tag{6}$$

which, in the absence of the dependence of $|\psi_{\ell^+\ell^-}\rangle$ upon $k_\perp$, would result in a δ functionlike behavior in configuration space. The authors of Ref. [106] chose to regularize this singularity by deleting the entire divergent term. Instead, a numerically superior subtraction scheme is obtained by only removing its limit as $k_\perp$ or $k_\perp'\to\infty$,

$$G_{2,\mathrm{reg}}=G_2+\left\{\frac{\alpha}{\pi}\frac{2}{x+x'-2xx'}\delta_{J_z,0}\right\},\tag{7}$$

which retains part of the term (including x and x' dependence). This scheme removes the strongest Λ dependence of ${}^1S_0$ states in both QED [25,148] and QCD [120] models. It is important to note that the $\boldsymbol{k}_\perp$ dependence of $|\psi_{\ell^+\ell^-}\rangle$ varies with α, and therefore it should be anticipated that the strength of this apparent divergence should also depend upon α. With this regularization scheme, the model allows for taking the $\Lambda \to \infty$ limit, albeit with a regularization dependence determined by mathematical, rather than purely physical, considerations.

Much of the previous work on QED with DLCQ has focused upon the unphysically large value $\alpha = 0.3$. In this regime, QED perturbative calculations can potentially become unreliable. We use this strong coupling value of α to study flavor mixing. New to this work, we investigate the approach to the physical $\mathcal{O}(10^{-2})$ value of the QED coupling constant.

III. RESULTS

Previous work has given results sensitive to numerical artifacts, limiting the reliability of the results that could be obtained. To overcome some of these limitations, we have produced a new numerical code, TMSWIFT (True Muonium Solver With Front-form Techniques), which is available online [149]. This code uses the parallel eigenvalue-solver package SLEPc [150], both to increase the number of Fock states and to decrease the time of calculation. TMSWIFT allows an arbitrary number of flavors, each specified by a distinct mass m_i, cutoff Λ, and discretization numbers N_μ and N_θ (although throughout this work we will fix $N_\mu = N_\theta = N$). Different discretization schemes are available in TMSWIFT for exploration of numerical errors and efficiency. Our code also allows easy implementation of new effective interactions (e.g., from $|\gamma\gamma\rangle$ states). These improvements have also allowed us to investigate lower values of α, where the extrapolation to $\Lambda, N \to \infty$ becomes more difficult. In order to examine these limits, except for Sed. III E which explicitly studies multiple-flavor effects, we restrict ourselves to the case of single-flavor true muonium.

In this section, we explore a number of properties of true muonium, dedicating a subsection to each: the invariant squared mass M_n^2, the ground-state HFS, the singlet and triplet wave functions, the decay constants, and multiflavor effects.

A. Invariant squared mass

With larger N and improved regularization, we found it possible to fit the energy levels, M_n^2, to Padé approximants of second order. To perform these fits, we first fit the N dependence for each value of Λ for which simulations were computed,

$$M^2(N,\Lambda) = \frac{M^2(\Lambda) + \frac{b}{N} + \frac{c}{N^2}}{1 + \frac{d}{N} + \frac{e}{N^2}}. \tag{8}$$

Then, the final $N \to \infty$ and $\Lambda \to \infty$ results can be obtained from a second fit to

$$M^2(\Lambda) = \frac{M_\infty^2 + \frac{f}{\Lambda} + \frac{g}{\Lambda^2}}{1 + \frac{h}{\Lambda} + \frac{i}{\Lambda^2}}. \tag{9}$$

These functions are well defined separately in the $N \to \infty$ and $\Lambda \to \infty$ limits, and therefore one can extract the continuum- and cutoff-independent values, M_∞^2. While in principle the entire data set could be simultaneously fit in N and Λ, the large cancellations that can occur between Padé coefficients, and the large number of parameters to fit in practice, make the process more difficult, and initial conditions for the fit must be carefully chosen to avoid local minima of the fits. Moreover, the two parameters have different origins: N is a numerical artifact, while Λ is a theoretical artifact. By fitting separately, these issues are largely avoided. Results for the ground-state singlet and triplet states are tabulated in Table I.

TABLE I. Extrapolated results for the bound-state invariant squared mass M^2 in units of m_μ^2, and the decay constants f_V, f_P in units of m_μ, for a range of α values. The column labeled $C_{\mathrm{HFS,LF}}$ is the computed hyperfine coefficient C_{HFS} from Eq. (13). The column labeled $C_{\mathrm{HFS,ET}}$ is the instant-form prediction for C_{HFS} from Eq. (14).

α	$M^2(1^1S_0)$	$f_V(1^1S_0)$	$M^2(1^3S_1)$	$f_P(1^3S_1)$	$C_{\mathrm{HFS,LF}}$	$C_{\mathrm{HFS,ET}}$
0.01	3.99989993(3)	$4.18(10) \times 10^{-5}$	3.99989996(3)	$3.893(6) \times 10^{-5}$	0.76(77)	0.5834
0.02	3.9995997(2)	$1.1(4) \times 10^{-4}$	3.9996002(2)	$1.088(7) \times 10^{-4}$	0.79(42)	0.5837
0.03	3.9990987(4)	$2.05(9) \times 10^{-4}$	3.999101(2)	$1.93(6) \times 10^{-4}$	0.74(34)	0.5841
0.04	3.998397(4)	$3.15(5) \times 10^{-4}$	3.998404(5)	$3.07(7) \times 10^{-4}$	0.76(56)	0.5847
0.05	3.9974914(4)	$4.466(2) \times 10^{-4}$	3.9975098(3)	$3.95(2) \times 10^{-4}$	0.74(2)	0.5855
0.07	3.995068(3)	$7.404(7) \times 10^{-4}$	3.9951351(8)	$5.908(5) \times 10^{-4}$	0.7(4)	0.5877
0.1	3.98987(6)	$1.273(2) \times 10^{-3}$	3.990137(3)	$9.16(3) \times 10^{-4}$	0.67(2)	0.5922
0.2	3.9576(6)	$3.9(2) \times 10^{-3}$	3.9614(5)	$1.9(2) \times 10^{-3}$	0.6(2)	0.6204
0.3	3.8996(6)	$1.02(3) \times 10^{-2}$	3.91538(4)	$2.39(2) \times 10^{-3}$	0.49(2)	0.6735

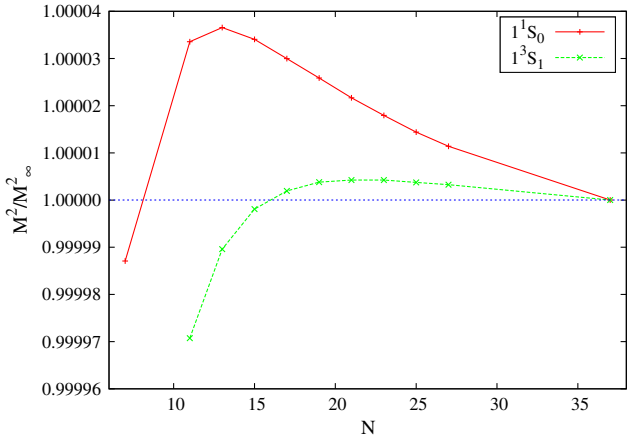

FIG. 1. Example of the dependence of M^2 upon N, normalized to the continuum and infinite limit for $\alpha = 0.2$, $\Lambda = 5m_\mu\alpha$.

An example of the dependence of M^2 upon N is shown in Fig. 1 for a fixed value of Λ and α. This dependence is qualitatively the same for all values of α and Λ. As can be seen, with increasing N, M^2 at first rises to a peak and then decreases toward a continuum value. The location of this peak is found to be proportional to $1/\alpha^2$ and linear in Λ. It is therefore more difficult to numerically simulate small α and large Λ, because any results that only sample to the left of the peaks systematically overestimate M^2, by not respecting that the functions decrease to the right of the peaks. From Fig. 1 it can also be seen that the triplet state reaches its (smaller) maximum at a larger N. It is also empirically found that, while the singlet state peaks at lower N, the variance of M^2 is much larger. With this understanding of the space of N, α, and Λ, one can study the approach to the perturbative regime of α. The analytic, instant-form values of M to $\mathcal{O}(\alpha^4)$ are given for 1^1S_0 and 1^3S_1 by [151]

$$M^2_{1^1S_0} = \left(2m - \frac{1}{4}m\alpha^2 - \frac{21}{64}m\alpha^4\right)^2, \tag{10}$$

$$M^2_{1^3S_1} = \left(2m - \frac{1}{4}m\alpha^2 + \frac{49}{192}m\alpha^4\right)^2. \tag{11}$$

Since $m = 1$ in our units, to test these formulas, one can fit to

$$M^2(\alpha) = (N_0 + N_2\alpha^2 + N_4\alpha^4 + N_4\alpha^5)^2. \tag{12}$$

From the Fock space considered in our model, a perturbative calculation should not have any higher-order contributions, but one could anticipate a possible $\mathcal{O}(\alpha^5)$ term due to the contributions of higher-order terms arising from our nonperturbative procedure and regularization scheme. The results of the fit are found in Table II.

Comparing the singlet-state results to Eqs. (10), one sees that TMSWIFT reproduces within uncertainty the $\mathcal{O}(\alpha^4)$ calculation over the entire range of α. Extracting possible higher-order coefficients would be possible by increasing N beyond what has been presented here. In contrast, for the triplet state, only the terms up to α^2 of Eqs. (11) are correctly reproduced. The α^4 coefficient reproduced the anticipated sign, but it is larger than the result of the instant-form calculation. Additionally, there is a large, unanticipated α^5 coefficient. Such results are indicative of issues in the annihilation channel, which affects only the triplet at this order.

B. Hyperfine splitting

To study these effects further, one can check how accurately our front-form model reproduces the expected instant-form results through the hyperfine coefficient, which is defined as

$$C_{\mathrm{HFS}} \equiv \frac{E_{\mathrm{HFS}}}{m_\mu\alpha^4} = \frac{\sqrt{M^2(1^3S_1)} - \sqrt{M^2(1^1S_0)}}{m_\mu\alpha^4}. \tag{13}$$

If all Fock states were included in our model, then the full known $\mathcal{O}(\alpha^7)$ instant-form prediction of E_{HFS} of Ref. [4] could be compared to our results. But because of our Fock-state truncations, there is a mismatch in the higher-order contributions. Since we can only extract up to $\mathcal{O}(\alpha^4)$, it is useful to compare to the leading-order value of $C_{\mathrm{HFS}} = \frac{7}{12}$.

Our model would be expected to partially resum the relativistic corrections from the single-photon exchange and annihilation diagrams. Therefore, we present the values of C_{HFS} given by the exact Dirac-Coulomb solutions [152],

$$\begin{aligned} C_{\mathrm{HFS}} &= \frac{1}{m_\mu\alpha^4}\left(\frac{E_F}{\sqrt{1-\alpha^2}[2\sqrt{1-\alpha^2}-1]}\right) \\ &= \frac{7}{12}\left(1 + \frac{3}{2}\alpha^2 + \frac{17}{8}\alpha^4 + \mathcal{O}(\alpha^6)\right), \end{aligned} \tag{14}$$

where $E_F = \frac{7}{12}m_\mu\alpha^4$ is the lowest-order HFS of true muonium. If higher precision could be attained, these effects might be resolvable, but at the current levels they are not yet visible.

Previous results for C_{HFS} at $\alpha = 0.3$ without the regularization term are found in Table 4.2 of Ref. [110] and can be calculated from the results found in Ref. [62]. The C_{HFS} obtained in these works appears to have a logarithmic singularity in the singlet state, indicating that no $\Lambda \to \infty$ limit could be taken. The severity of the divergence can be seen in Ref. [110], where C_{HFS} rises from ≈ 0.313 at $\Lambda = m_f$ to ≈ 1.27 at $\Lambda = 18m_f$. In contrast, we find that for our regularization scheme, C_{HFS} is finite because the two energy levels are finite in the $N \to \infty$ and $\Lambda \to \infty$ limits. The numerical results in Table I are roughly consistent over

TABLE II. Parameters of Eq. (12) for the singlet and triplet states of true muonium, fit over two ranges of α. The $\mathcal{O}(\alpha^4)$ perturbative predictions are $N_0 = 2$, $N_2 = -\frac{1}{4}$, $N_{4,1^1S_0} = -\frac{21}{64} \approx -0.328$, $N_{4,1^3S_1} = \frac{49}{192} \approx 0.255$. The expected value of N_5 is unknown but is anticipated to be small. Reported uncertainties result solely from the fitting procedure.

E_n	α	N_0	N_2	N_4	N_5
1^1S_0	[0.01, 0.3]	1.99999998(2)	−0.2500(2)	−0.37(5)	−0.04(21)
	[0.01, 0.1]	1.999999990(2)	−0.25004(2)	−0.35(2)	0.08(10)
1^3S_1	[0.01, 0.3]	1.99999998(2)	−0.24990(8)	0.39(3)	−0.78(8)
	[0.01, 0.1]	1.999999979(6)	−0.24993(5)	0.38(3)	−0.60(26)

the entire range of α, albeit with large uncertainty. While the results are finite, we find that the central values are systematically larger than the anticipated $\frac{7}{12} \approx 0.58$, being in the range 0.7–0.8 except for $\alpha = 0.3$, where observables approach their asymptotic values more slowly due to changes in the wave function large-$\boldsymbol{k}$ dependence, as discussed in the next section.

Clearly, a disagreement is seen between the two instant-form predictions and the results on the light front. Previously, several authors [102,106,110] have also pointed out that the correct value of C_{HFS} is best obtained for $\Lambda \approx m\alpha$, and the results from TMSWIFT support this point of view. Unfortunately, the divergences spoil this agreement at larger Λ, necessitating renormalization. The larger splitting in the infinite-Λ limit can be understood thusly: Although the regularization procedure developed allows for extrapolation to $\Lambda \to \infty$, the Λ dependences of the singlet and triplet states are different, as was seen in [25], leading to an asymptotic HFS that, while finite, is larger than the known result.

These results are in contrast to the situation in which the annihilation-channel interaction is excluded. Choosing the intermediate case of $\alpha = 0.1$, we performed an exploratory search with a smaller number of simulations. In this case, we found in the continuum and infinite-Λ limits that $C_{\mathrm{HFS}} = 0.35(11)$, in agreement with the anticipated value at leading order of $C_{\mathrm{HFS}} \approx 0.333$. A similar small study for $\alpha = 0.3$ with $J_z = 1$ also found a value of $C_{\mathrm{HFS}} \approx 0.75$, indicating that both the dynamical and the instantaneous annihilation interactions are affected. This evidence further suggests that the annihilation-channel interaction is the source of the discrepancies.

To understand why the annihilation channel gives trouble, it is useful to recall how this term is included in instant form. In standard, perturbative nonrelativistic calculations, these contributions in coordinate space are represented as a contact term $\propto \delta^{(3)}(\mathbf{r})$; therefore, in momentum space these terms are very sensitive to large momenta, and imposing a cutoff Λ prevents these momenta from contributing. Furthermore, we have already seen that obtaining numerical results for large Λ is complicated by the need to include much larger N than is currently possible. Put together, these facts indicate that regularization and renormalization are more complicated in the annihilation channel.

C. Wave functions

In order to understand the effect of the regularization term on the effective interaction, we have studied the large-μ behavior of the wave functions. The momentum-space wave function obtained from the nonrelativistic Schrödinger equation is

$$\Psi(\boldsymbol{k}) = \frac{\sqrt{8}}{\pi} \frac{1}{(1+\boldsymbol{k}^2)^2}, \tag{15}$$

where the instant-form 3-momentum carries units of Bohr momentum $\frac{1}{2}m\alpha$. It is known that higher-order corrections to the interaction lead to a modified power law, changing the large-$\boldsymbol{k}$ power scaling from the nonrelativistic value of -4. Since according to Eq. (5) $\boldsymbol{k}$ is linear in μ, for our studies it suffices to compute the dependence upon α at large μ. The large-μ behavior is parametrized as

$$\Psi(\mu) = a\mu^{-\kappa}, \tag{16}$$

where $\kappa = 4$ is the result for the nonrelativistic Schrödinger equation.

In [106], it was found that for $\alpha_{\mathrm{QED}} = 1/137$, the large-$\mu$ behavior of the $\uparrow\downarrow$ singlet wave function is $\kappa = 4.0$, in agreement with expectations, and that for $\alpha = 0.3$ the behavior is $\kappa = 2.5$. We believe this large reduction in κ is related to the strong Λ dependence found in [106,110]. To further understand the relation between regularization and κ, we fit the large-μ tail of our wave functions to Eq. (16) with the results for a selected few values of α shown in Fig. 2. In all of these cases, we have implemented our regularization subtraction scheme. The values of κ for $\alpha = 0.01, 0.07$ appear to show only small deviations from the nonrelativistic value, consistent with [106]. In contrast, our value of $\kappa = 3.59$ for $\alpha = 0.3$ is dramatically larger than found in the unregulated results of [106]. Since the large-μ tail decays much faster than in [106], the contribution of any potentially divergent terms will be reduced, explaining why the results of [25] showed such a dramatic improvement.

Using our entire set of α results, it is possible to study the effect of varying α upon κ. Shown in Fig. 3 are the extracted values of κ for both the dominant $\uparrow\downarrow$ component of the singlet state and the subleading $\uparrow\uparrow$ component. We have

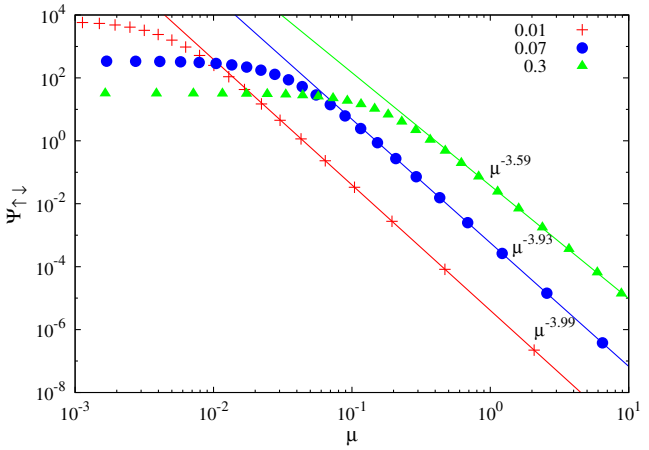

FIG. 2. Dependence of the $\uparrow\downarrow$ component of the 1^1S_0 state upon μ for a fixed value of $x = 0.5$ for different values of α. The points indicate the numerical results, and the solid lines are the fits used to extract κ.

also obtained values of κ for a smaller set of α without using our regularization scheme. Because the regularization term is only needed for G_2, it makes sense that only the $\uparrow\downarrow$ has a dramatic change in its α dependence by the introduction of the regularization term, whereas the $\uparrow\uparrow$ wave functions are mostly unaffected.

D. Decay constants

In addition to the invariant masses, the decay constants offer an interesting observable that can be extracted from the wave functions. They also serve as a good test bed for understanding how the properties of the wave function are affected by regularization and renormalization. The decay constants in the vector V and pseudoscalar P channels are defined by

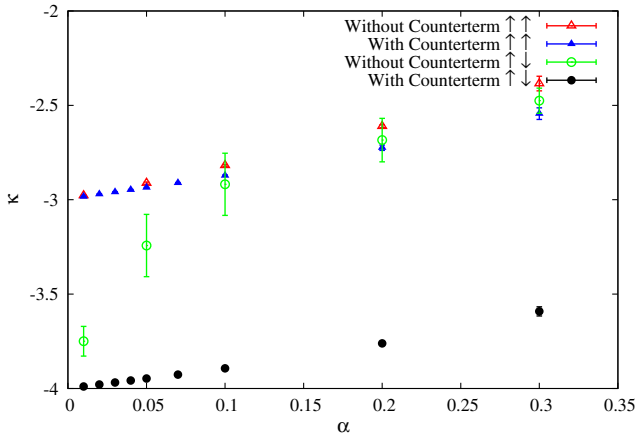

FIG. 3. κ vs α for the $\uparrow\uparrow$ and $\uparrow\downarrow$ components of the 1^1S_0 state. Open (closed) symbols indicate results excluding (including) the regularization term.

TABLE III. Fit parameters of Eq. (19) for the vector decay constant f_V of the singlet state and the pseudoscalar decay constant f_P of the triplet state for two ranges of α. N has units of m. The leading-order perturbative prediction is $\beta = 3/2$.

f_i	α	N	β
f_V	[0.01, 0.3]	0.0412(9)	1.510(7)
	[0.01, 0.1]	0.0411(3)	1.509(3)
f_P	[0.01, 0.3]	0.022(3)	1.37(4)
	[0.01, 0.1]	0.0240(8)	1.394(10)

$$\langle 0|\bar{\psi}\gamma^\mu\psi|V(p),\lambda\rangle = \epsilon^\mu_\lambda m_V f_V,$$
$$\langle 0|\bar{\psi}\gamma^\mu\gamma^5\psi|P(p)\rangle = ip^\mu f_P, \tag{17}$$

where $\epsilon^\mu_\lambda(p)$ is the polarization vector for the boson, and $\lambda = 0, \pm 1$. In front-form field theory, the decay constants can be computed directly from the $+$ components of these currents which, following Refs. [120,153], are given for QED bound states by

$$f_{V(P)} = \int \frac{\mathrm{d}x}{\sqrt{x(1-x)}} \frac{\mathrm{d}^2\boldsymbol{k}_\perp}{(2\pi)^3} [\psi^J_{J_z=0}(\boldsymbol{k}_\perp, x, \uparrow\downarrow) \mp \psi^J_{J_z=0}(\boldsymbol{k}_\perp, x, \downarrow\uparrow)], \tag{18}$$

where the vector (pseudoscalar) decay constant is given by the difference (sum) of the two terms in the equation. Taking the component wave functions from TMSWIFT calculations, it is possible to obtain f_V for the singlet state and f_P for the triplet state as a function of α. Like the invariant masses, the decay constants are found to be well fit to the functional form of Eq. (8), and therefore infinite-cutoff values for them can be obtained. These results can be found in Table I.

For the decay constants, one expects $f_i \propto |\psi_i(0)|/\sqrt{M_i}$, which suggests a $\alpha^{3/2}$ power law at leading order. To check this prediction, a fit is performed to the function

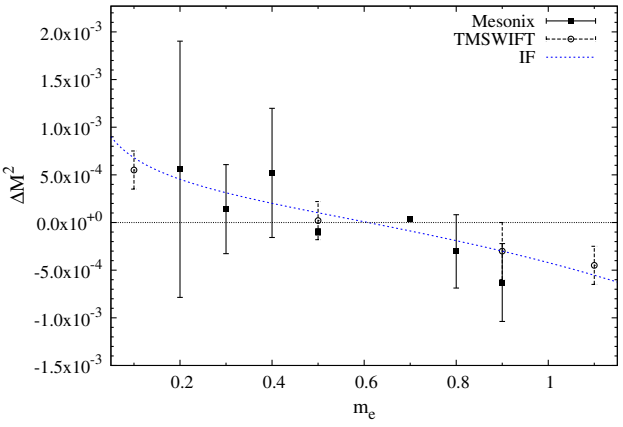

FIG. 4. ΔM^2 corrections from a second flavor of leptons to true muonium as a function of the second flavor's mass m_e. Errors are estimated from the numerical fit alone.

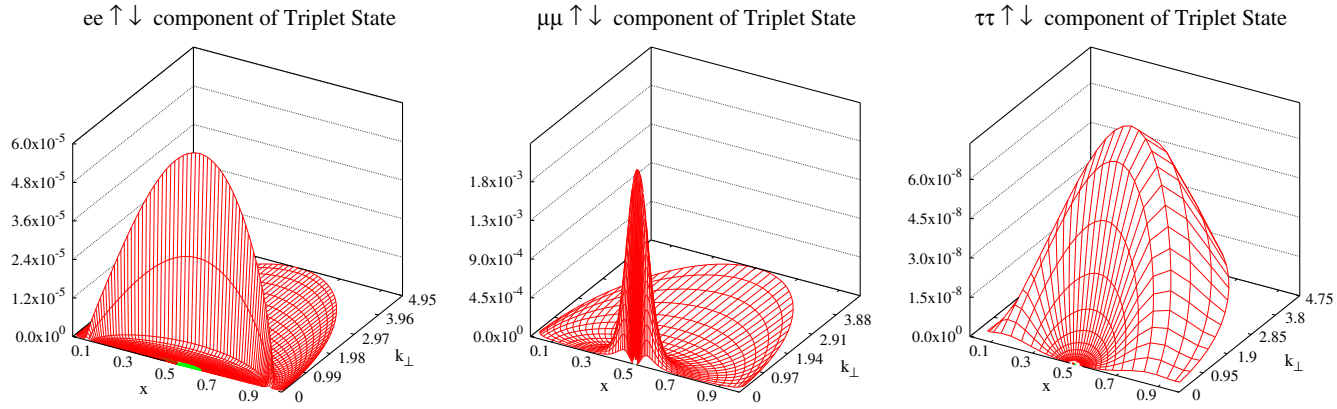

FIG. 5. The $1^3S_1^0$ probability density of the $\uparrow\downarrow$ components of (left) e^+e^-, (center) $\mu^+\mu^-$, and (right) $\tau^+\tau^-$, with $J_z = 0$, as a function of x and $k_\perp$, for $\alpha = 0.3$, $m_\mu/m_e = m_\tau/m_\mu = 2$, $\Lambda_i = 5\alpha m_i$, and $N_\mu = 37$, $N_\tau = 31$, $N_e = 71$.

$$f_i(\alpha) = N\alpha^\beta, \tag{19}$$

and the results are exhibited in Table III.

Similar to the invariant masses, the f_V values for the singlet state seem to reproduce the perturbative form to leading order very well over for all values of α. The agreement between f_P for the triplet state shows a poorer agreement, especially for large α, where the inclusion of the annihilation channel enables higher-order corrections to the decay rate.

E. Multiple-flavor effects

True muonium is acutely sensitive to the effects of multiple flavors. The large mass difference $m_\mu/m_e \approx 207$ causes electronic loop corrections to be the largest corrections to the spectrum of true muonium. Additionally, the ratio $m_\tau/m_\mu \approx 16$ is small enough to produce appreciable effects on the system at $\mathcal{O}(\alpha^5)$. While the vacuum polarization in the exchange diagrams is neglected by our model, it is possible to study these effects in the annihilation channel.

Previous results [25] found large, nonlinear N and Λ_e dependence from the electronic contribution, even for the unphysically large ratio of $m_\mu/m_e = 2$. With TMSWIFT, we have been able to further study this dependence. Numerical limitations prevent the collection of a sufficiently large number of simulations to fit to Padé approximants. Instead, we fix $\alpha = 0.3$, $N_\mu = 21$, $\Lambda_\mu = 10$ (Λ_i is given in units of $m_i\alpha$), and then obtain estimates for ΔM^2 (the shift of squared mass eigenvalues due to the inclusion of additional lepton flavors) by averaging over the ranges $N_e \in [27, 35]$ and $\Lambda_e \in [1, 35]$.

We have been able to further reduce the uncertainty through two new ideas. First, simulations were made using two different discretization schemes, Gauss-Legendre and Curtis-Clenshaw. The use of two discretization schemes for the same N_e allows us to explore the effects of discretization on the continuum electron states with smaller N.

TABLE IV. Integrated probability for each flavor in the true muonium $1^3S_1^0$ state. The parameters used are $\alpha = 0.3$, $m_\mu/m_e = m_\tau/m_\mu = 2$, $\Lambda_i = 5\alpha m_i$, and $N_\mu = 37$, $N_\tau = 31$, $N_e = 71$.

Flavor	$\int \mathrm{d}x\mathrm{d}^2\boldsymbol{k}_\perp P(x, k_\perp)$
$\lvert\mu^+\mu^-\rangle$	0.992
$\lvert e^+e^-\rangle$	0.008
$\lvert\tau^+\tau^-\rangle$	$\approx 1.2 \times 10^{-5}$

Additionally, f_P is a sensitive probe of the coupling of electron continuum states to the bound state. Empirically, we find that if the value of f_P differs by more than 10% from the single-flavor case, the simulation has sampled the continuum in an inaccurate way and can be excluded from the average.

Producing results for the physical value of the electron mass remains difficult numerically because of the large separation of scales. Our results for the corrections to true muonium from electronic loops in the annihilation channel are shown in Fig. 4, compared to the anticipated instant-form result, and the previous results of [25]. One can see that TMSWIFT's parallel implementation, while still numerically limited, can produce better agreement with the instant form than found in [25], with smaller uncertainty.

TMSWIFT has also been written to allow for an arbitrary number of flavors. We present here results from a three-flavor true muonium model, albeit with unphysical ratios $m_\mu/m_e = m_\tau/m_\mu = 2$, keeping $\alpha = 0.3$. In Fig. 5 are shown the probability densities of the $\uparrow\downarrow$ components of each flavor for the triplet state. In Table IV we present the relative probability for each component in this case.

IV. DISCUSSION AND CONCLUSION

In this work we have presented results for the invariant mass and decay constants of the true muonium system. For the first time, we have gone beyond the case $\alpha = 0.3$ and

shown that the approach to α_{QED} is possible with sufficient numerical resources. The purpose of this program is not to produce energy levels competitive in the weak-field limit with perturbative calculations. Instead, our goals in calculating at α_{QED} are to produce true muonium wave functions that can be used in relativistic situations, and as to provide an independent check on our methods, allowing one to be confident in the strong-field predictions. Furthermore, using our previously developed regularization scheme, the simultaneous limits of $N \to \infty$ and $\Lambda \to \infty$ have been taken and stable results found. These values have been compared to the instant-form perturbative calculations, and reasonable agreement has been obtained. Finally, initial studies have been undertaken to compute the fully nonperturbative contribution to the bound state arising from additional flavors, both lighter and more massive than the muon. Improved agreement with instant-form predictions have been obtained for a range of masses of a second flavor, and simulations of the three-flavor model have been produced.

Currently, work is underway to include the $|\gamma\gamma\rangle$ state and the pair of states $|\ell\bar{\ell}\ell\bar{\ell}\rangle$ and $|\ell\bar{\ell}\ell'\bar{\ell}'\rangle$, which are required for gauge invariance. These corrections are crucial for precision true muonium predictions and are a necessary step for QCD bound states as well.

Proper renormalization of the Hamiltonian is the remaining obstacle. In order to make accurate predictions, the Λ dependence found in this work must be systematically removed, which involves not just including new Fock sectors, but imposing gauge invariance at each stage. A proper implementation of charge renormalization and the running of the coupling α should address a large part of the issue. A first step in this direction would focus upon implementing a renormalized vacuum polarization into the effective interactions. With a robust renormalization scheme, multiple values of Λ would not be needed to take the $\Lambda \to \infty$, greatly reducing the numerical effort to produce reliable results. With TMSWIFT, Fock-space limitations have been greatly decreased. This improvement allows for the implementation of explicit Fock-state renormalization methods like Pauli-Villars regulators [56–58] and sector-dependent counterterms [52,55]. Using the exchange properties of leptons could further reduce the number of basis states, similar to the methods used in Ref. [154] for bosons. More time-intensive renormalization schemes like the Hamiltonian-flow method [61,62] also become viable with a parallel implementation.

ACKNOWLEDGMENTS

This work was supported by the National Science Foundation under Grants No. PHY-1068286 and No. PHY-1403891. This work used the Extreme Science and Engineering Discovery Environment (XSEDE), which is supported by National Science Foundation Grant No. ACI-1053575, and the ASU Physics Computing Cluster.

[1] S. J. Brodsky and R. F. Lebed, Phys. Rev. Lett. **102**, 213401 (2009).
[2] U. Jentschura, G. Soff, V. Ivanov, and S. G. Karshenboim, Phys. Rev. A **56**, 4483 (1997).
[3] U. Jentschura, G. Soff, V. Ivanov, and S. G. Karshenboim, Phys. Lett. B **424**, 397 (1998).
[4] H. Lamm, Phys. Rev. D **91**, 073008 (2015).
[5] G. Bennett *et al.* (Muon G-2 Collaboration), Phys. Rev. D **73**, 072003 (2006).
[6] A. Antognini *et al.*, Science **339**, 417 (2013).
[7] R. Aaij *et al.* (LHCb Collaboration), Phys. Rev. Lett. **113**, 151601 (2014).
[8] R. Aaij *et al.* (LHCb Collaboration), Phys. Rev. Lett. **115**, 111803 (2015); **115**, 159901(E) (2015).
[9] D. Tucker-Smith and I. Yavin, Phys. Rev. D **83**, 101702 (2011).
[10] H. Lamm, arXiv:1509.09306.
[11] H. Lamm, Phys. Rev. D **92**, 055007 (2015).
[12] L. Nemenov, Yad. Fiz. **15**, 1047 (1972).
[13] J. Moffat, Phys. Rev. Lett. **35**, 1605 (1975).
[14] E. Holvik and H. A. Olsen, Phys. Rev. D **35**, 2124 (1987).
[15] G. Kozlov, Sov. J. Nucl. Phys. **48**, 167 (1988).
[16] I. Ginzburg, U. Jentschura, S. G. Karshenboim, F. Krauss, V. Serbo, and G. Soff, Phys. Rev. C **58**, 3565 (1998).
[17] N. Arteaga-Romero, C. Carimalo, and V. Serbo, Phys. Rev. A **62**, 032501 (2000).
[18] Y. Chen and P. Zhuang, arXiv:1204.4389.
[19] A. Banburski and P. Schuster, Phys. Rev. D **86**, 093007 (2012).
[20] S. Ellis and J. Bland-Hawthorn, Phys. Rev. D **91**, 123004 (2015).
[21] A. Celentano (HPS Collaboration), J. Phys. Conf. Ser. **556**, 012064 (2014).
[22] A. Benelli (DIRAC Collaboration), EPJ Web Conf. **37**, 01011 (2012).
[23] P. Chliapnikov, Report No. DIRAC-NOTE-2014-05, 2014.
[24] L. L. Nemenov and V. D. Ovsyannikov, Phys. Lett. B **514**, 247 (2001).
[25] H. Lamm and R. F. Lebed, J. Phys. G **41**, 125003 (2014).
[26] H. Lamm and R. F. Lebed, Few-Body Syst. **57**, 663 (2016).
[27] S. Weinberg, Phys. Rev. **150**, 1313 (1966).
[28] P. A. M. Dirac, Rev. Mod. Phys. **21**, 392 (1949).
[29] S. J. Brodsky, H.-C. Pauli, and S. S. Pinsky, Phys. Rep. **301**, 299 (1998).
[30] J. B. Kogut and D. E. Soper, Phys. Rev. D **1**, 2901 (1970).

[31] N. E. Ligterink and B. L. G. Bakker, Phys. Rev. D **52**, 5954 (1995).
[32] S.-J. Chang, R. G. Root, and T.-M. Yan, Phys. Rev. D **7**, 1133 (1973).
[33] T.-M. Yan, Phys. Rev. D **7**, 1760 (1973).
[34] S.-J. Chang and T.-M. Yan, Phys. Rev. D **7**, 1147 (1973).
[35] B. L. G. Bakker, M. van Iersel, and F. Pijlman, Few-Body Syst. **33**, 27 (2003).
[36] B. L. G. Bakker, M. A. DeWitt, C.-R. Ji, and Y. Mishchenko, Phys. Rev. D **72**, 076005 (2005).
[37] A. Misra and S. Warawdekar, Phys. Rev. D **71**, 125011 (2005).
[38] B. L. G. Bakker, J. K. Boomsma, and C.-R. Ji, Phys. Rev. D **75**, 065010 (2007).
[39] S. M. Patel and A. Misra, Phys. Rev. D **82**, 125024 (2010).
[40] G. P. Lepage and S. J. Brodsky, Phys. Rev. D **22**, 2157 (1980).
[41] B. D. Jones and R. J. Perry, Phys. Rev. D **55**, 7715 (1997).
[42] B. D. Jones, R. J. Perry, and S. D. Głazek, Phys. Rev. D **55**, 6561 (1997).
[43] B. D. Jones, High-energy Physics and Cosmology, in *Proceedings, 25th Coral Gables International Conference on Orbis Scientiae, Miami Beach, USA, 1997*, (Plenum, New York, 1997), pp. 201–207.
[44] B. D. Jones, Ph. D. thesis, Ohio State University, 1997.
[45] S. D. Głazek, A. Harindranath, S. Pinsky, J. Shigemitsu, and K. Wilson, Phys. Rev. D **47**, 1599 (1993).
[46] M. Mangin-Brinet, J. Carbonell, and V. A. Karmanov, Phys. Rev. D **64**, 125005 (2001).
[47] M. Mangin-Brinet, J. Carbonell, and V. A. Karmanov, Phys. Rev. C **68**, 055203 (2003).
[48] P. P. Srivastava and S. J. Brodsky, Phys. Rev. D **66**, 045019 (2002).
[49] S. D. Głazek and K. G. Wilson, Phys. Rev. D **48**, 5863 (1993).
[50] V. A. Karmanov, J. Carbonell, and M. Mangin-Brinet, AIP Conf. Proc. **603**, 271 (2001).
[51] J. Carbonell, M. Mangin-Brinet, and V. A. Karmanov, arXiv:nucl-th/0202042.
[52] V. A. Karmanov, J. F. Mathiot, and A. V. Smirnov, Phys. Rev. D **77**, 085028 (2008).
[53] V. A. Karmanov, J. F. Mathiot, and A. V. Smirnov, Phys. Rev. D **82**, 056010 (2010).
[54] V. A. Karmanov, J. F. Mathiot, and A. V. Smirnov, Nucl. Phys. B, Proc. Suppl. **199**, 35 (2010).
[55] V. A. Karmanov, J. F. Mathiot, and A. V. Smirnov, Phys. Rev. D **86**, 085006 (2012).
[56] S. S. Chabysheva and J. R. Hiller, Phys. Rev. D **81**, 074030 (2010).
[57] S. S. Chabysheva and J. R. Hiller, Phys. Rev. D **82**, 034004 (2010).
[58] M. Yu. Malyshev, S. A. Paston, E. V. Prokhvatilov, and R. A. Zubov, Int. J. Theor. Phys. **54**, 169 (2015).
[59] J. R. Hiller, Few-Body Syst. **57**, 557 (2016).
[60] S. S. Chabysheva and J. R. Hiller, arXiv:1506.05429.
[61] E. L. Gubankova, H.-C. Pauli, and F. J. Wegner, arXiv:hep-th/9809143.
[62] E. L. Gubankova and G. Papp, arXiv:hep-th/9904081.
[63] E. Gubankova, C.-R. Ji, and S. R. Cotanch, Phys. Rev. D **62**, 074001 (2000).
[64] E. Gubankova, C.-R. Ji, and S. R. Cotanch, Phys. Rev. D **62**, 125012 (2000).
[65] H. C. Pauli and S. J. Brodsky, Phys. Rev. D **32**, 2001 (1985).
[66] M. Sawicki, Phys. Rev. D **33**, 1103 (1986).
[67] M. Sawicki, Phys. Rev. D **32**, 2666 (1985).
[68] A. Harindranath and J. P. Vary, Phys. Rev. D **36**, 1141 (1987).
[69] A. Harindranath and J. P. Vary, Phys. Rev. D **37**, 1076 (1988).
[70] A. Harindranath and J. P. Vary, Phys. Rev. D **37**, 1064 (1988).
[71] K. Hornbostel, S. J. Brodsky, and H. C. Pauli, Phys. Rev. D **41**, 3814 (1990).
[72] J. B. Swenson and J. R. Hiller, Phys. Rev. D **48**, 1774 (1993).
[73] T. Eller, H. C. Pauli, and S. J. Brodsky, Phys. Rev. D **35**, 1493 (1987).
[74] T. Heinzl, S. Krusche, and E. Werner, Phys. Lett. B **275**, 410 (1992).
[75] G. McCartor, Z. Phys. C **52**, 611 (1991).
[76] G. McCartor, Z. Phys. C **64**, 349 (1994).
[77] G. McCartor, Int. J. Mod. Phys. A **12**, 1091 (1997).
[78] Y. Nakawaki and G. McCartor, Prog. Theor. Phys. **103**, 161 (2000).
[79] S. Strauss and M. Beyer, Phys. Rev. Lett. **101**, 100402 (2008).
[80] S. Strauss and M. Beyer, Prog. Part. Nucl. Phys. **62**, 535 (2009).
[81] S. Strauss and M. Beyer, Nucl. Phys. B, Proc. Suppl. **199**, 160 (2010).
[82] J. R. Hiller, Phys. Rev. D **43**, 2418 (1991).
[83] B. van de Sande, Phys. Rev. D **54**, 6347 (1996).
[84] U. Trittmann, Nucl. Phys. **B587**, 311 (2000).
[85] U. Trittmann, Phys. Rev. D **66**, 025001 (2002).
[86] U. Trittmann, Phys. Rev. D **92**, 085021 (2015).
[87] S. Pinsky and U. Trittmann, Phys. Rev. D **62**, 087701 (2000).
[88] J. R. Hiller, S. Pinsky, and U. Trittmann, Phys. Rev. D **64**, 105027 (2001).
[89] J. R. Hiller, S. S. Pinsky, and U. Trittmann, Phys. Rev. D **65**, 085046 (2002).
[90] J. R. Hiller, S. S. Pinsky, and U. Trittmann, Phys. Rev. D **66**, 125015 (2002).
[91] J. R. Hiller, S. S. Pinsky, and U. Trittmann, Phys. Lett. B **541**, 396 (2002).
[92] J. R. Hiller, S. S. Pinsky, and U. Trittmann, Nucl. Phys. **B661**, 99 (2003).
[93] J. R. Hiller, S. S. Pinsky, and U. Trittmann, Phys. Rev. D **67**, 115005 (2003).
[94] J. R. Hiller, M. Harada, S. S. Pinsky, N. Salwen, and U. Trittmann, Phys. Rev. D **71**, 085008 (2005).
[95] J. R. Hiller, S. S. Pinsky, N. Salwen, and U. Trittmann, Phys. Lett. B **624**, 105 (2005).
[96] J. R. Hiller, S. Pinsky, Y. Proestos, N. Salwen, and U. Trittmann, Phys. Rev. D **76**, 045008 (2007).
[97] U. Trittmann and S. S. Pinsky, Phys. Rev. D **80**, 065005 (2009).
[98] S. S. Pinsky and B. van de Sande, Phys. Rev. D **49**, 2001 (1994).

[99] S. S. Pinsky, B. van de Sande, and J. R. Hiller, Phys. Rev. D **51**, 726 (1995).
[100] C. M. Bender, S. Pinsky, and B. Van de Sande, Phys. Rev. D **48**, 816 (1993).
[101] J. R. Hiller, O. Lunin, S. Pinsky, and U. Trittmann, Phys. Lett. B **482**, 409 (2000).
[102] A. C. Tang, S. J. Brodsky, and H. C. Pauli, Phys. Rev. D **44**, 1842 (1991).
[103] L. C. L. Hollenberg, Discretized light cone quantization applied to QCD in four-dimensions, 1991, http://alice.cern.ch/format/showfull?sysnb=0129374.
[104] M. Kaluža and H. C. Pauli, Phys. Rev. D **45**, 2968 (1992).
[105] F. Wölz, Master's thesis, Heidelberg, 1990.
[106] M. Krautgärtner, H. C. Pauli, and F. Wölz, Phys. Rev. D **45**, 3755 (1992).
[107] A. C. Kalloniatis and H. C. Pauli, Z. Phys. C **60**, 255 (1993).
[108] M. Krautgärtner, Ph. D. thesis, Heidelberg, 1992.
[109] F. Wölz, Ph. D. thesis, Heidelberg, 1995.
[110] U. Trittmann and H.-C. Pauli, arXiv:hep-th/9704215.
[111] U. Trittmann, arXiv:hep-th/9705072.
[112] U. Trittmann and H. C. Pauli, Nucl. Phys. B, Proc. Suppl. **90**, 161 (2000).
[113] J. P. Vary, H. Honkanen, J. Li, P. Maris, S. J. Brodsky, A. Harindranath, G. F. de Téramond, P. Sternberg, E. G. Ng, and C. Yang, Phys. Rev. C **81**, 035205 (2010).
[114] X. Zhao, H. Honkanen, P. Maris, J. P. Vary, and S. J. Brodsky, Few-Body Syst. **52**, 339 (2012).
[115] P. Maris, P. Wiecki, Y. Li, X. Zhao, and J. P. Vary, Acta Phys. Pol. B Proc. Suppl. **6**, 321 (2013).
[116] X. Zhao, A. Ilderton, P. Maris, and J. P. Vary, Phys. Rev. D **88**, 065014 (2013).
[117] X. Zhao, A. Ilderton, P. Maris, and J. P. Vary, Phys. Lett. B **726**, 856 (2013).
[118] D. Chakrabarti, X. Zhao, H. Honkanen, R. Manohar, P. Maris, and J. P. Vary, Phys. Rev. D **89**, 116004 (2014).
[119] X. Zhao, H. Honkanen, P. Maris, J. P. Vary, and S. J. Brodsky, Phys. Lett. B **737**, 65 (2014).
[120] Y. Li, P. Maris, X. Zhao, and J. P. Vary, Phys. Lett. B **758**, 118 (2016).
[121] H.-C. Pauli, A. C. Kalloniatis, and S. S. Pinsky, Phys. Rev. D **52**, 1176 (1995).
[122] S. Dalley and B. van de Sande, Nucl. Phys. B, Proc. Suppl. **53**, 827 (1997).
[123] B. van de Sande and S. Dalley, Neutrino Mass, Dark Matter, Gravitational Waves, Monopole Condensation, and Light Cone Quantization, in *Proceedings, International Conference, Orbis Scientiae 1996, Miami Beach, USA* (Springer, New York, 1996), pp. 241–250.
[124] S. Dalley, AIP Conf. Proc. **494**, 45 (1999).
[125] B. van de Sande and M. Burkardt, Phys. Rev. D **53**, 4628 (1996).
[126] M. M. Brisudova, R. J. Perry, and K. G. Wilson, Phys. Rev. Lett. **78**, 1227 (1997).
[127] D. Chakrabarti and A. Harindranath, Phys. Rev. D **64**, 105002 (2001).
[128] G. F. de Téramond and S. J. Brodsky, Phys. Rev. Lett. **102**, 081601 (2009).
[129] G. F. de Téramond and S. J. Brodsky, AIP Conf. Proc. **1257**, 59 (2010).
[130] S. J. Brodsky, G. F. de Téramond, and A. Deur, Phys. Rev. D **81**, 096010 (2010).
[131] G. F. de Téramond and S. J. Brodsky, AIP Conf. Proc. **1296**, 128 (2010).
[132] S. J. Brodsky, G. F. De Téramond, and H. G. Dosch, Phys. Lett. B **729**, 3 (2014).
[133] S. J. Brodsky, G. F. de Téramond, H. G. Dosch, and J. Erlich, Phys. Rep. **584**, 1 (2015).
[134] G. F. de Téramond, H. G. Dosch, and S. J. Brodsky, Phys. Rev. D **91**, 045040 (2015).
[135] S. J. Brodsky, A. Deur, G. F. de Téramond, and H. G. Dosch, Int. J. Mod. Phys. Conf. Ser. **39**, 1560081 (2015).
[136] H. G. Dosch, G. F. de Téramond, and S. J. Brodsky, Phys. Rev. D **92**, 074010 (2015).
[137] H. G. Dosch, G. F. de Téramond, and S. J. Brodsky, Phys. Rev. D **91**, 085016 (2015).
[138] S. S. Chabysheva and J. R. Hiller, Phys. Lett. B **711**, 417 (2012).
[139] S. S. Chabysheva and J. R. Hiller, arXiv:1203.0250.
[140] B. Elliott, S. S. Chabysheva, and J. R. Hiller, Phys. Rev. D **90**, 056003 (2014).
[141] A. Misra, Phys. Rev. D **50**, 4088 (1994).
[142] A. Misra, Phys. Rev. D **53**, 5874 (1996).
[143] A. Misra, Phys. Rev. D **62**, 125017 (2000).
[144] J. D. More and A. Misra, Phys. Rev. D **86**, 065037 (2012).
[145] J. D. More and A. Misra, Phys. Rev. D **87**, 085035 (2013).
[146] H. C. Pauli, Perspectives of Strong Coupling Gauge Theories, in *Proceedings, International Workshop, SCGT'96, Nagoya, Japan, 1996* (World Scientific, Singapore, 1997), pp. 342–352.
[147] V. A. Karmanov, Nucl. Phys. **A362**, 331 (1981).
[148] P. Wiecki, Y. Li, X. Zhao, P. Maris, and J. P. Vary, Phys. Rev. D **91**, 105009 (2015).
[149] H. Lamm, https://github.com/operabed/tmswift.git, 2016.
[150] V. Hernandez, J. E. Roman, and V. Vidal, ACM Trans. Math. Softw. **31**, 351 (2005).
[151] H. Bethe and E. Salpeter, *Quantum Mechanics of One- and Two-Electron Atoms* (Academic, New York, 1957), p. 170.
[152] G. Breit, Phys. Rev. **35**, 1477 (1930).
[153] T. Branz, T. Gutsche, V. E. Lyubovitskij, I. Schmidt, and A. Vega, Phys. Rev. D **82**, 074022 (2010).
[154] S. S. Chabysheva and J. R. Hiller, Phys. Rev. E **90**, 063310 (2014).